nt. J. Electrochem. Sci., 13 **(2018)** 8723 – 8735, doi: 10.20964/2018.09.50

International Journal of
ELECTROCHEMICAL
SCIENCE
www.electrochemsci.org

Electrochemical Corrosion Behaviour of Carbon Steel in Acidic Media in Presence of Mn_2O_3 Nanoparticles Synthesized at Different pH

R. Najjar[1], *A. M. Abdel-Gaber*[1,*], *R. Awad*[2]

[1] Department of Chemistry, Faculty of Science, Beirut Arab University, P.O. Box 11-5020 Riad El Solh 11072809 - Beirut, Lebanon
[2] Department of Physics, Faculty of Science, Beirut Arab University, P.O. Box 11-5020 Riad El Solh 11072809 - Beirut, Lebanon
[*]E-mail: ashrafmoustafa@yahoo.com; a.abdelgaber@bau.edu.lb

Received: 10 May 2018 / *Accepted:* 28 June 2018 / *Published:* 5 August 2018

The effect of Mn_2O_3 nanoparticles synthesized at different pH by co-precipitation method on the electrochemical corrosion behaviour of carbon steel in 0.5 M hydrochloric acid was inspected by potentiodynamic polarization and electrochemical impedance spectroscopy (EIS) techniques. The corrosion behaviour of carbon steel in 0.5 M HCl, 0.5 M H_3PO_4 and 0.5 M H_2SO_4 was also examined in presence of 20 ppm Mn_2O_3 nanoparticles. Mn_2O_3 nanoparticles prepared at pH 10 to 13 were characterized by X-ray diffraction, XRD, transmission electron microscopy, TEM, and Fourier transform infrared analyses, FTIR. Electrochemical impedance spectroscopy measurements showed that the dissolution process takes place under activation control. Potentiodynamic polarization curves showed that Mn_2O_3 nanoparticles slightly enhance the corrosion resistance of carbon steel in acidic solutions. The efficiency was found to increase with decreasing pH at which Mn_2O_3 nanoparticles were synthesized. Mn_2O_3 nanoparticles synthesized at pH 10 has a better effect in 0.5 M HCl than in 0.5 M H_2SO_4 or 0.5 M H_3PO_4.

Keywords: Corrosion, steel, Mn_2O_3, polarization, impedance.

1. INTRODUCTION

Transition metal oxide nanoparticles have been highlighted in many fields going from bioengineering to automotive engineering. [1]. They have been utilized as catalysts [2-3], sensors and anodes for ion batteries. In addition, in smart windows, electrochemical supercapacitors and as an antiferromagnetic thin film [4-5]. Newly, nanoparticles such as zirconium oxide, titanium dioxide, have

been of great interest beneficial to enhance the efficiency of several inhibitors to protect metals [6-7]. Manganese oxide, Mn_2O_3, has a higher oxidation state [8] and can be used as an environmentally friendly catalyst for removing nitrogen oxide and carbon monoxide from waste gases [9] and has a biogenic and bioscience application [10]. It is considered as magnetic nanoparticle used in magnetic data storage as well as magnetic resonance imaging (MRI). Currently, the focus of the research is to replace the toxic compound [11] with environmentally friendly inhibitors. Among numerous metals, mild steel is considered as a structural material of choice due to its versatility [12], inexpensive and material properties required for different applications. In industry, acid cleaning, descaling [13], and acid pickling [14] are usually used to remove scale and rust. However, the problem of mild steel corrosion is very serious conducive to a premature deterioration and failure of engineering components, which increases repair and maintenance cost. Furthermore, one of the most efficient way to preserve industrial facilities [15] and protect metal is the use of an adequate inhibitor.

Previous publications discussed the electrochemical behavior of NiO or SnO_2 nanoparticles doped superconductor in sodium sulphate solution [16, 17]. Therefore, it is worth to study the effect of nanoparticles present in solution on the electrochemical behavior of metals that are used in daily life applications. This work aims to test the effect of Mn_2O_3 nanoparticles synthesized at different pH by co-precipitation method on the electrochemical corrosion behavior of steel in 0.5 M HCl and to compare its efficiency with that in 0.5 M H_2SO_4 and 0.5 M H_3PO_4.

2. EXPERIMENTAL TECHNIQUES

2.1. Mn_2O_3 Nanoparticles preparation.

Mn_2O_3 nanoparticles were prepared by co-precipitation method at different pH ranging from 10 to 13. Manganese chloride tetrahydrate; ethylenediaminetetraacetic acid, EDTA; sodium hydroxide, NaOH; and distilled water were used for the preparation. All chemicals were purchased from Sigma Aldrich chemical company. The reaction was performed by dissolving 30 g of Manganese chloride tetrahydrate ≥98%, and 4.42 g ethylenediaminetetraacetic acid in 200 ml distilled water. The obtained solution was magnetically stirred at room temperature and 4M NaOH was added dropwise to adjust the solution pH to 10, 11, 12 or 13 using the Ohaus pH meter. The precipitation occurred by heating the prepared solution at 70˚C for 2 h. The products were filtered, washed with distilled water, then dried at 90˚C for 16 h in air. The dried ingots were heated in the muffle furnace at the rate of 4˚C/ min at 550˚C for 6 h.

2.2. Solutions preparation.

The acid solutions 0.5 M HCl, 0.5 M H_2SO_4 and 0.5 M H_3PO_4 were prepared by dilution of analytical grade acid 37% HCl, 96% H_2SO_4, and 86% H_3PO_4 respectively with distilled water.

2.3. Nanoparticles characterization

The structure and particle size of Mn_2O_3 nanoparticles were characterized using X-ray diffraction analysis with an advance X-Ray powder diffractometer (Bruker D8) with Cu-K_α radiation (λ = 1.54056 Å) in the range $20^o \leq 2\theta \leq 80^o$. The X-ray tube used was a copper tube operating at 30 kV and 30 mA.

Furthermore, transmission electron microscopy (TEM) micrograph was applied to identify the crystalline size using Jeol transmission electron microscope, operated at 80 kV providing magnification from 100x to 250000x and a resolution of 0.2 nm.

Fourier transform infrared analyses of the samples were performed using a model FTIR 410 JASCO spectrometer in transmission mode of range 4000-400 cm^{-1}.

2.4. Electrochemical tests.

A frequency response analyzer (FRA) / potentiostat provided from ACM instruments (UK) is used to study the Electrochemical impedance (EIS) and polarization measurements using an electrochemical cell, enclosing three electrodes: platinum electrode, saturated calomel electrode, and a working electrode. The carbon steel used for constructing the working electrode was of the following chemical composition (wt. %) C, 0.21; S, 0.04; Mn, 2.5; P, 0.04; Si, 0.35; balance Fe [18]. The working electrode was abraded with 300, 600 and 800 grade emery papers, washed with distilled water and ethanol and then inserted into the cell. The frequency range for EIS measurements was 0.1 to $3x10^4$ Hz with an applied potential signal amplitude of ± 10 mV around the rest potential. Polarization curves measurements were performed at a scan rate of 30mV/min within ±250 mV around equilibrium potential. The temperature of test solution was kept constant at 30ºC using WiseCircu water bath (Germany). To test the reliability and reproducibility of the measurements, duplicate experiments were performed in each case of the same conditions.

3. RESULTS AND DISCUSSION

3.1. Samples characterization.

Typical XRD diffraction patterns of Mn_2O_3 nanoparticles prepared at pH 10-13 are shown in Figure 1.

In the XRD spectrum, comparing the observed peaks to the standard peaks of pure Mn_2O_3 (JCPDS 41-1442) indicate that all samples show well indexed cubic phase. The average crystallite size of the nanoparticles was estimated using Debye-Scherer's formula:

$D = k\lambda / \beta\cos(\theta)$

where k represents the shape factor (0.9), β is the instrument broadening width with instrumental correction at half size and θ is the peak position. The particle sizes were found in the range 65.91-110.48 nm respectively, for Mn_2O_3 nanoparticles synthesized at different pH, Table 1.

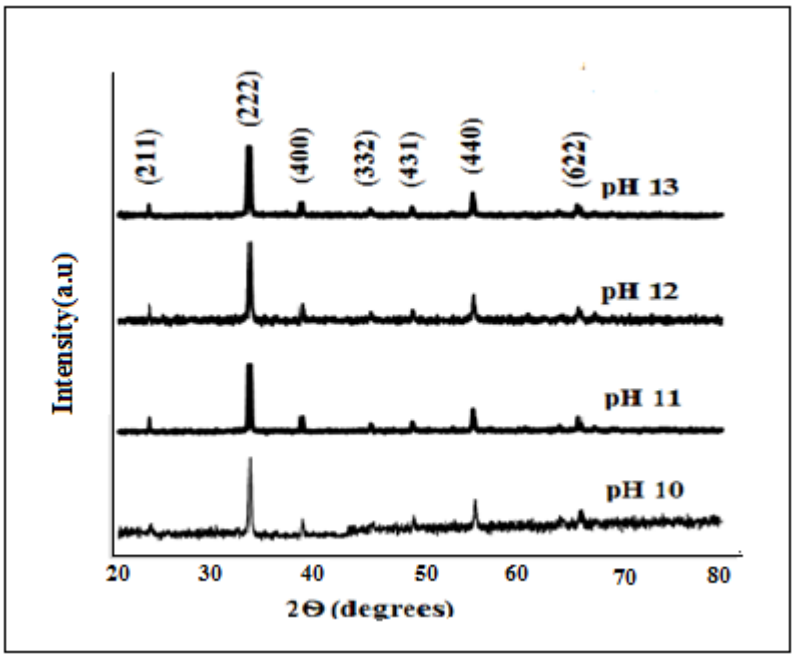

Figure 1. XRD spectrum with (hkl) values of Mn_2O_3 nanoparticles synthesized at different pH.

Table 1. Particle size of Mn_2O_3 nanoparticles synthesized at different pH.

pH	**10**	**11**	**12**	**13**
Particle size(nm)	110.48	106.81	77.01	65.91

It is observed that the increasing pH decreases the particle size. These data are in a good agreement with that observed from TEM image for Mn_2O_3 nanoparticles synthesized at different pH, Figure 2. The figure shows significant change of particle size, morphology, and extent of aggregation state. The performed morphology consists of a cubic shape nanoparticle. It is well known that the initial pH values influenced the balance of ions in the solution as well as the crystal growth pattern [19].

Fourier transform infrared (FTIR) spectrum of Mn_2O_3 synthesized at different pH is shown in Figure 3. The absorption peaks 593.73 cm^{-1} and 519.09 cm^{-1} relate to the stretching vibration of Mn-O and Mn-O-Mn bonds [20] during the synthesis of Mn_2O_3 nanoparticles and the peaks at 3500 $cm^{-1}$and 1632.17 cm^{-1} is attributed respectively to stretching and bending vibrations of the OH group of water molecules that remained in the sample. It is clearly observed that the pH change does not affect the position of peaks in the IR spectra of Mn_2O_3 nanoparticles.

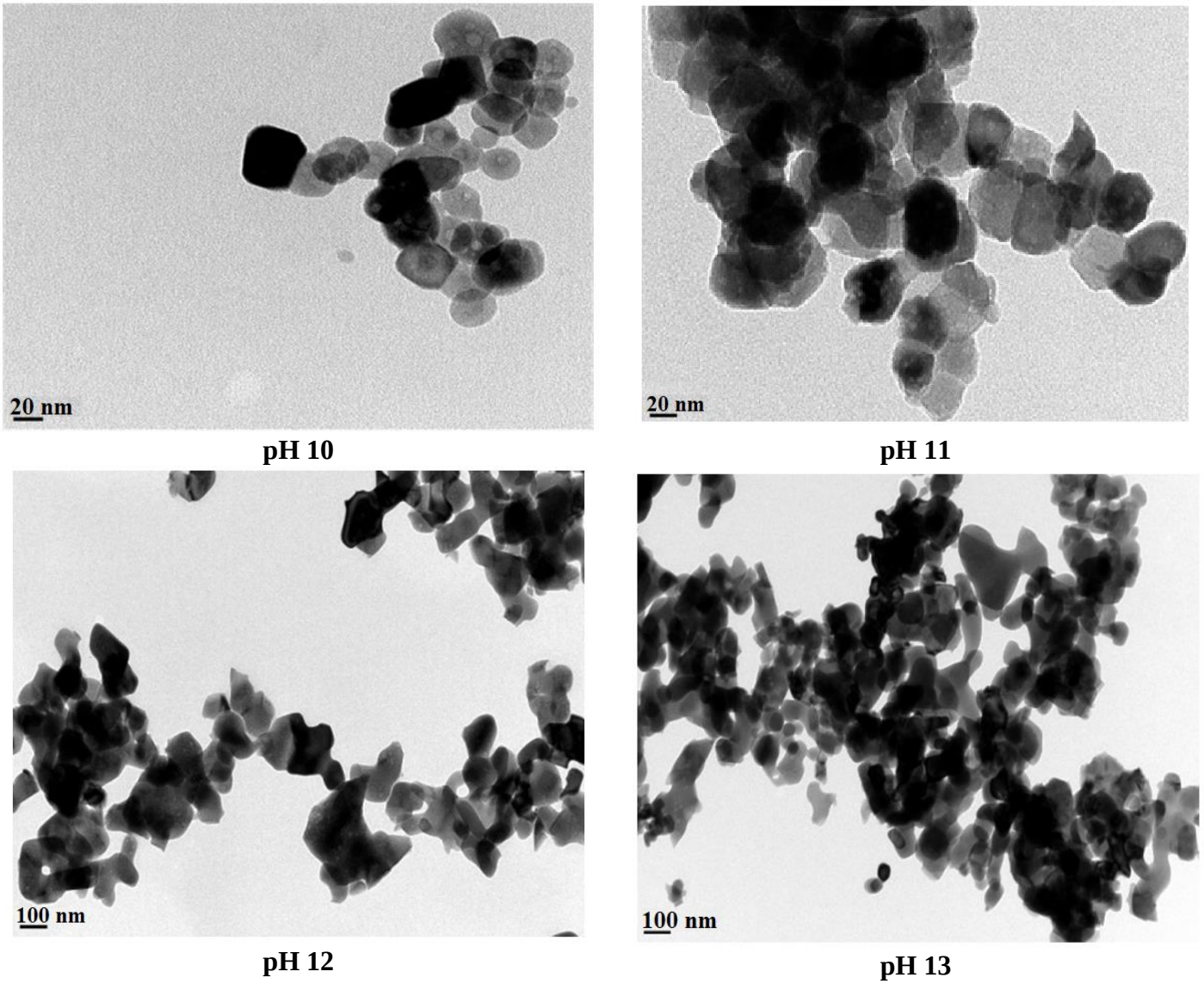

Figure 2. TEM images of Mn_2O_3 nanoparticles synthesized at different pH

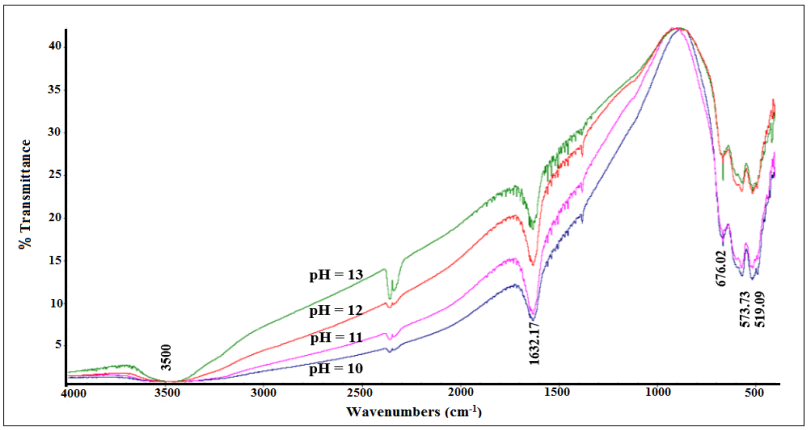

Figure 3. FTIR spectrum of Mn_2O_3 synthesized at different pH.

3.2. Electrochemical Studies.

3.2.1. EIS measurements of the effect of Mn_2O_3 nanoparticles concentrations

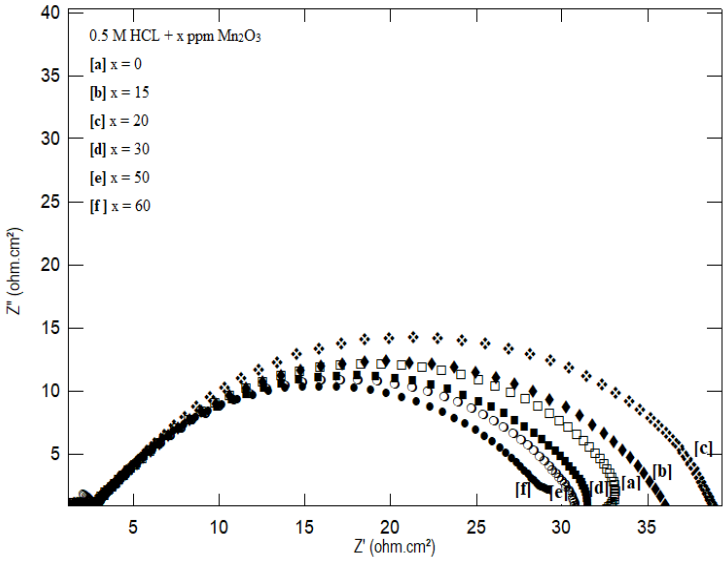

Figure 4. Nyquist impedance plots for steel in 0.5 M HCl in the absence and presence of different concentrations of Mn_2O_3 nanoparticles.

Figure 4 shows the Nyquist impedance responses of steel in 0.5 M HCl in the absence and presence of different concentrations of Mn_2O_3 nanoparticles synthesized at pH=10. As seen, the obtained semicircle increases in size with increasing Mn_2O_3 nanoparticles concentration up to 20 ppm. Afterwards, it decreases for further additions. It is generally known that, the size of the semicircle and the corrosion rate are inversely proportional. Thus, 20 ppm displays the lowest corrosion rate. For this reason, 20 ppm was chosen for further study.

3.2.2. The effect of of Mn_2O_3 nanoparticles synthesized at different pH in 0.5M HCl

3.2.2.1. Open circuit potential measurements.

The variation of the open circuit potential (OCP) with time for the steel electrode in 0.5 M HCl in the absence and presence of 20 ppm Mn_2O_3 nanoparticles synthesized at pH 10-13, Figure 5, is measured to define domains of corrosion. The attainment of a constant potential after 20 minutes corresponding to the free corrosion of the steel. A slightly shifting of the potential of steel to more noble direction is detected with decreasing pH at which the nanoparticles were synthesized. This could be explained on the basis that Mn_2O_3 nanoparticles synthesized at low pH have larger size, Table 1, that cover more active anodic sites controlling the anodic process.

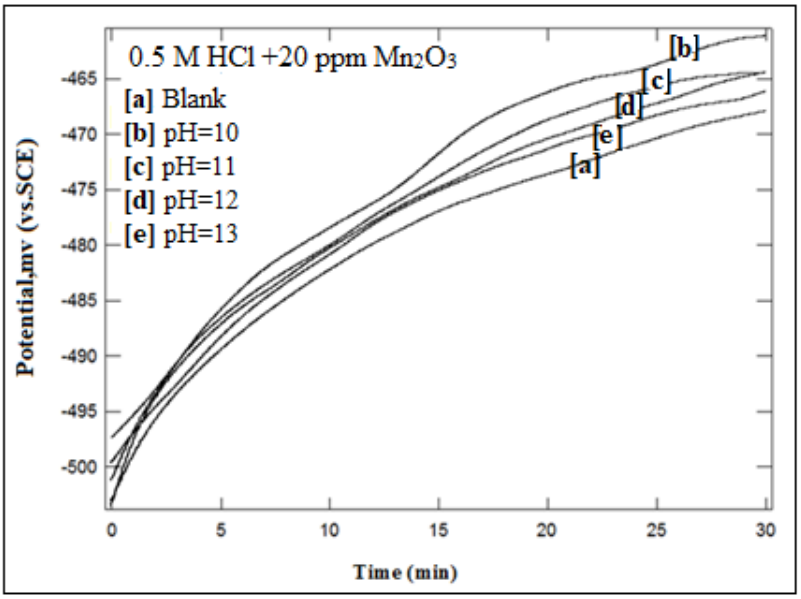

Figure 5. A variation of the open circuit potential with time for steel in 0.5 M HCl solution in the absence and presence of 20 ppm Mn_2O_3 nanoparticles synthesized at different pH.

3.2.2.2. Potentiodynamic polarization measurements.

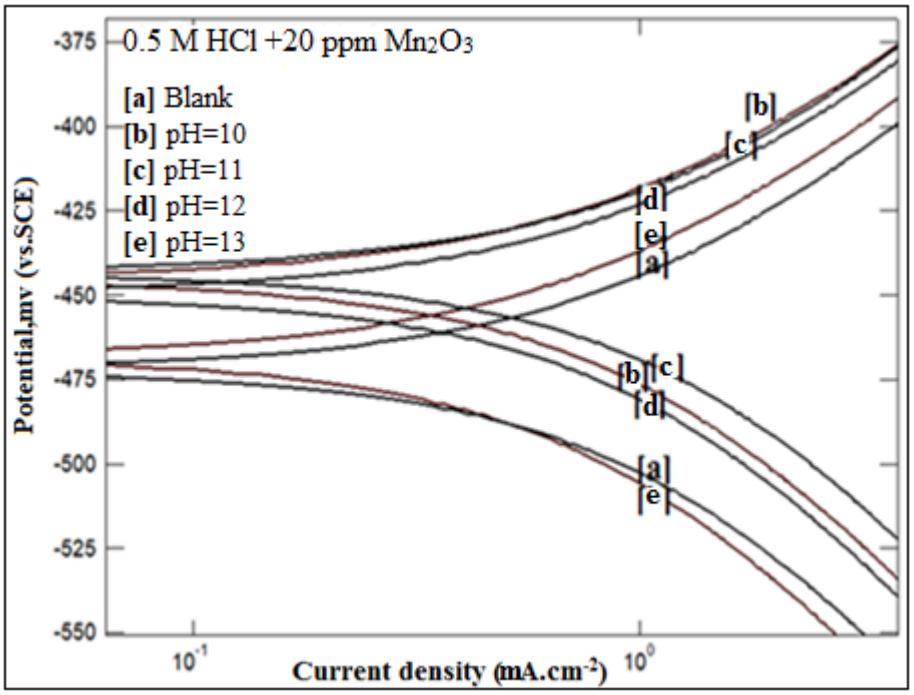

Figure 6. Potentiodynamic polarization curves for steel in 0.5 M HCl in the absence and presence of 20 ppm of Mn_2O_3 nanoparticles at different pH.

Potentiodynamic polarization curves presented in figure 6 show that the nanoparticles have an inhibiting effect on the anodic part of the polarization curves. The values of the electrochemical

parameters: corrosion potential (E_{corr}), corrosion current density, i_{corr}, anodic and cathodic Tafel slopes, β_a, and β_c are given in Table 2. The inhibition efficiency, %η, was calculated from $i_{corr.}$ using the formula :

$$\%\eta = [\, i_{corr} - i_{corr(inhibitor)})/\, i_{corr}] \times 100$$

Where i_{corr} and $i_{corr(inhibitor)}$ are the corrosion current density values in the absence and presence of Mn_2O_3 nanoparticles synthesized at different pH, respectively,

The displayed data show that the nanoparticles synthesized at low pH, which represents the highest nanoparticles size, have the lowest i_{corr} and highest %η. The slight variations in values of β_a and β_c indicate that the corrosion mechanism does not change in the presence of Mn_2O_3 nanoparticles.

Table 2. Electrochemical polarization parameters and %η for steel in 0.5M HCl in the absence and presence of 20 ppm Mn_2O_3 nanoparticles synthesized at different pH.

Mn_2O_3 nanoparticles	$-E_{corr}$ mV	β_a	β_C	i_{corr} mA/cm^2	%η
		mV.dec^{-1}			
Blank	461	101	130	0.685	-
pH 10	442	82	110	0.319	53.34
pH 11	441	85	112	0.432	36.93
pH 12	444	80	113	0.448	34.59
pH 13	438	86	120	0.527	23.06

3.2.2.2. Electrochemical impedance spectroscopy result

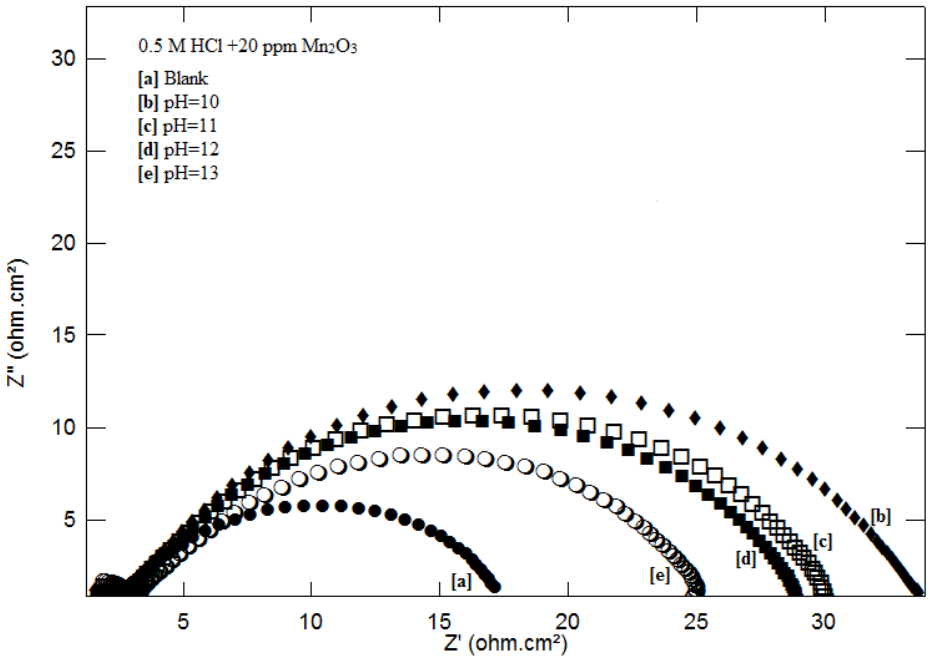

Figure 7. Nyquist Impedance plots of steel in 0.5 M hydrochloric acid in the absence and presence of Mn_2O_3 nanoparticles synthesized at different pH.

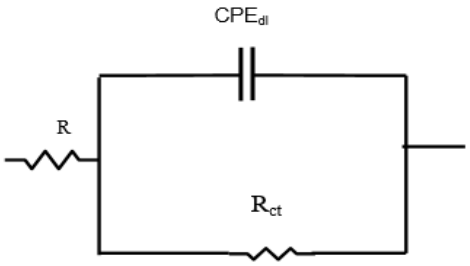

Figure 8. Electrochemical equivalent circuit used to fit the impedance.

The Nyquist impedance plots shown in Figure 7 indicate that the impedance response consisted of depressed semicircles of capacitive type whose size increases with decreasing the pH at which nanoparticles synthesized. The impedance spectra for different Nyquist plots were analyzed by fitting the experimental data to an equivalent circuit model in Figure 8 that includes the solution resistance R_s and constant phase element of the double layer (CPE_{dl}) which is placed in parallel to charge transfer resistance element, R_{ct} defined as the measure of electron transfer across the surface.

. The capacitances were implemented as a constant phase element (CPE) during analysis of the impedance plots. The CPE is defined by two values, Q and n. The impedance, Z, of CPE is presented by

$$Z_{CPE} = Q^{-1} (i\omega)^{-n}$$

where $i = (-1)^{1/2}$, ω is frequency in rad s^{-1}, $\omega = 2f\pi$ and f is the frequency in Hz. If n equals one, then Z_{CPE} is identical to that of a capacitor, $Z_{CPE} = (i\omega C)^{-1}$ where C is the ideal capacitance. For a non-homogeneous system, n values range from 0.9 to 1.

The values of R_s,, R_{ct} ,$C_{dl,}$ n and the inhibition efficiency (% η) for steel in 0.5 M Hydrochloric acid containing 20 ppm of Mn_2O_3 nanoparticles synthesized at different pH are given in Table 3.

Table 3. Electrochemical impedance parameters and % η for steel in 0.5M HCl in the absence and presence of 20 ppm of Mn_2O_3 nanoparticles synthesized at different pH.

Mn_2O_3 nanoparticles	Rs Ohm.cm^2	Rct Ohm.cm^2	Cdl μF/cm^2	n	% η
Blank	2.27	15.48	235	0.83	-
pH 10	2.99	34.84	328	0.85	55.6
pH 11	2.83	27.38	402	0.86	43.2
pH 12	2.74	26.54	473	0.87	41.4
pH 13	3.01	22.43	603	0.84	30.6

The data indicate that the increase in particle size that is associated the decrease in pH leads to increasing charge transfer resistance that and decreasing C_{dl}. This clarifies that the inhibition takes place through the adsorption mechanism [18].

The inhibition efficiency, % η was calculated from impedance measurements using the relation:

$\% \eta = [(R_{ct} - R_{cto}) / R_{ct}] \times 100$

where R_{cto} and R_{ct} are the charge transfer resistance of steel in 0.5 M Hydrochloric acid in the absence and presence of 20 ppm Mn_2O_3 nanoparticles synthesized at different pH. The variation of %η

obtained from electrochemical impedance measurements presented in Table 3 are in good agreement with that obtained from potentiodynamic polarization curves, Table 2.

3.3. Effect of 20 ppm Mn_2O_3 nanoparticles synthesized by co-precipitation method at pH 10 in 0.5M HCl, 0.5 M H_2SO_4 and 0.5 M H_3PO_4.

The previous part showed that Mn_2O_3 nanoparticles synthesized by co-precipitation method at pH 10 acquire the highest efficiency related to their highest particle size and lowest pH.

The aim of this part is to extend our study by comparing the inhibition efficiency of Mn_2O_3 nanoparticles synthesized at pH 10 in 0.5M HCl, 0.5 M H_2SO_4 and 0.5 M H_3PO_4. This will clarify the effect of acid anion on the inhibition efficiency Mn_2O_3 nanoparticles on the corrosion of steel.

Potentiodynamic polarization curves of mild steel in 0.5 M H_2SO_4 and 0.5 M H_3PO_4 in the absence and presence of 20 ppm Mn_2O_3 nanoparticles synthesized at pH 10 are shown in Figure 9.

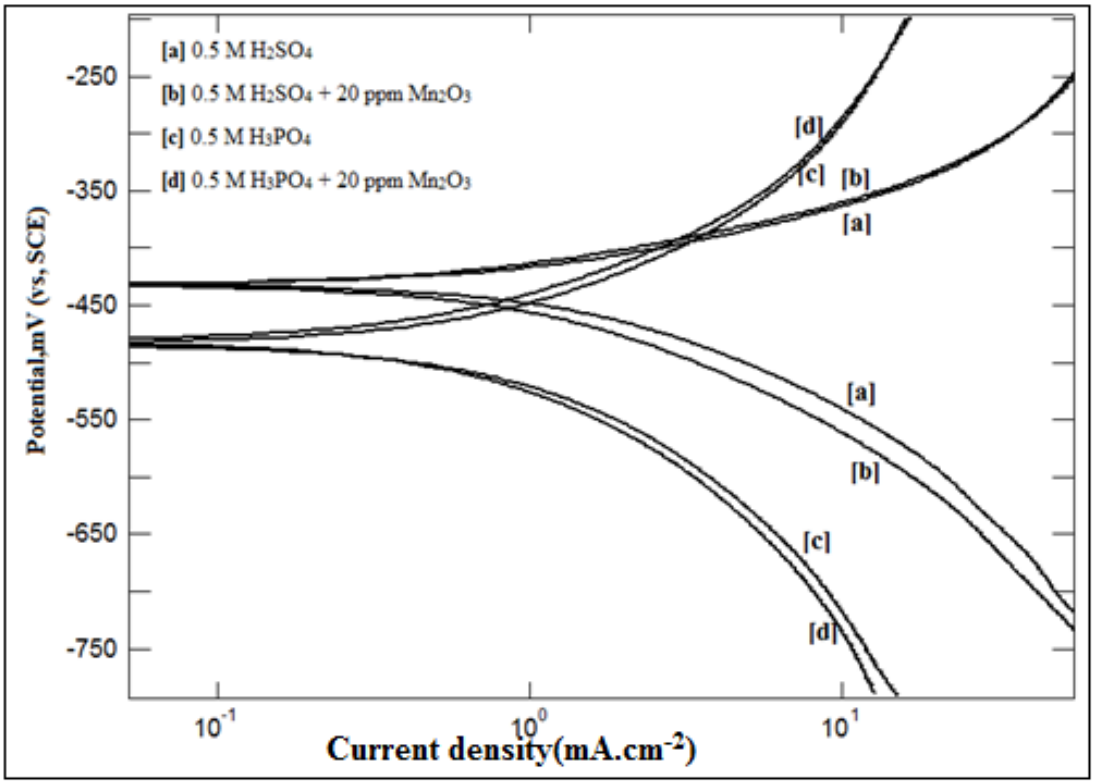

Figure 9. Potentiodynamic polarization curves of mild steel in 0.5 M H_2SO_4 and 0.5 M H_3PO_4 in the absence and presence of 20 ppm Mn_2O_3 nanoparticles synthesized at pH 10.

It is evident from the polarization curves that Mn_2O_3 nanoparticles inhibit the anodic dissolution of mild steel. The electrochemical polarization parameters of mild steel in in 0.5M HCl, 0.5 M H_2SO_4 and 0.5 M H_3PO_4 in the absence and presence of 20 ppm Mn_2O_3 nanoparticles synthesized at pH 10 are shown in Table 4.

Table 4. Electrochemical polarization parameters and % η for steel in 0.5M HCl, 0.5 M H_2SO_4 and 0.5 M H_3PO_4 in the absence and presence of 20 ppm of Mn_2O_3 nanoparticles synthesized at pH 10.

Acid	Mn_2O_3 nanoparticles	$-E_{corr}$ mV	β_a mV.dec^{-1}	β_C	i_{corr} mA/cm^2	% η
0.5M HCl	0.0 ppm	461	101	130	0.685	-
	20 ppm	442	82	110	0.319	53.4
0.5 M H_3PO_4	0.0 ppm	484	116	130	0.554	-
	20 ppm	475	99	134	0.4189	24.5
0.5 M H_2SO_4	0.0 ppm	424	67	119	1.090	-
	20 ppm	431	70	118	0.846	22.4

Analysis of the inhibition data reveals that inhibition efficiency increases in the order HCl > H_3PO_4> H_2SO_4.

Nyquist impedance plots of mild steel in 0.5 M H_2SO_4 and 0.5 M H_3PO_4 in the absence and presence of 20 ppm Mn_2O_3 nanoparticles synthesized at pH 10 are shown in Figure 10.

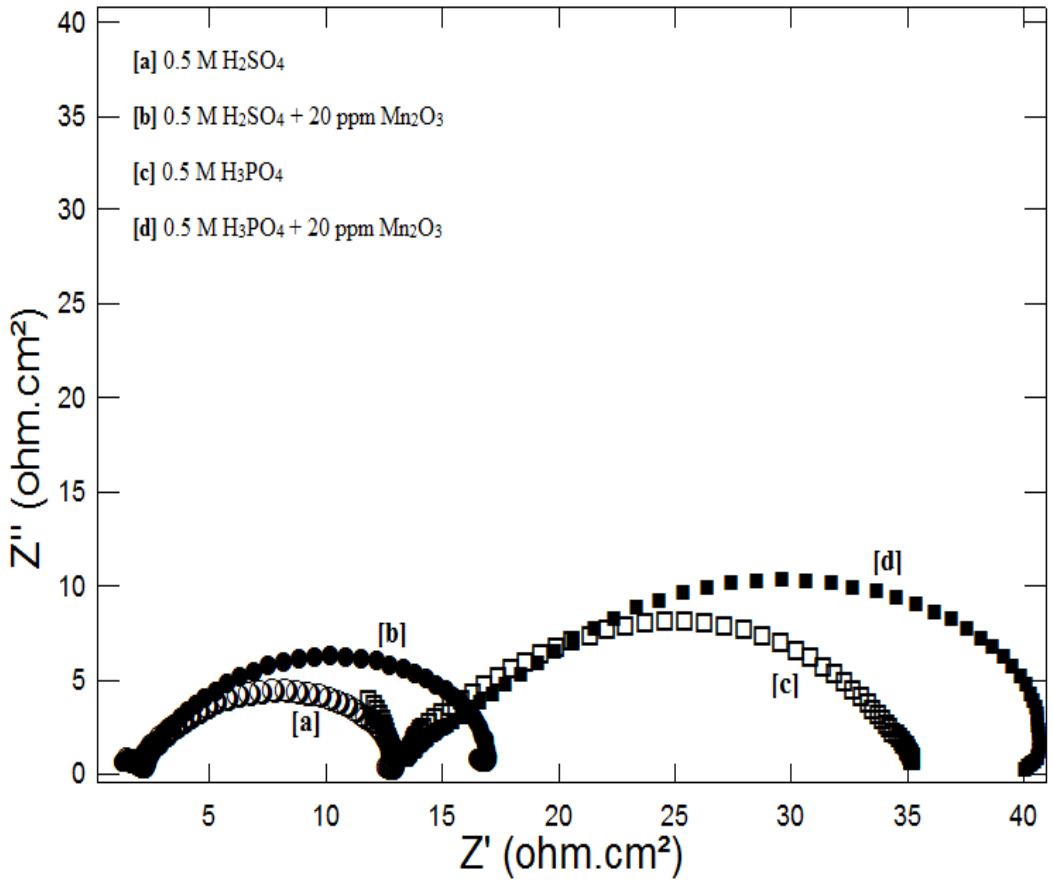

Figure 10. Nyquist impedance plots of mild steel in 0.5 M H_2SO_4 and 0.5 M H_3PO_4 in the absence and presence of 20 ppm Mn_2O_3 nanoparticles synthesized at pH 10 are shown in Figures10.

Table 5. Electrochemical impedance parameters and % η for steel in 0.5M HCl, 0.5 M H_2SO_4 and 0.5 M H_3PO_4 in the absence and presence of 20 ppm of Mn_2O_3 nanoparticles synthesized at pH 10.

Acid	Mn_2O_3 nanoparticles	Rs Ohm.cm^2	R_{ct} Ohm.cm^2	Q_{dl} μF/cm^2	n	% η
0.5M HCl	0.0 ppm	2.27	15.48	235.4	0.83	-
	20 ppm	2.99	34.84	327.5	0.85	55.6
0.5 M H_3PO_4	0.0 ppm	13.1	22.37	440.9	0.79	-
	20 ppm	12.7	30.88	427.2	0.75	27.6
0.5 M H_2SO_4	0.0 ppm	2.00	11.73	605.3	0.82	-
	20 ppm	2.03	15.74	518.1	0.86	25.5

It is noticeable from the plot that the impedance response has been significantly altered after the addition of Mn_2O_3 nanoparticles to the 0.5 M H_2SO_4 and 0.5 M H_3PO_4 solution.

The values of R_s, R_{ct}, $C_{dl,}$ n, and the inhibition efficiency (% η) of steel in 0.5M HCl, 0.5 M H_2SO_4 and 0.5 M H_3PO_4 in the absence and presence of 20 ppm Mn_2O_3 nanoparticles synthesized at pH 10 are given in table 5**.**

The results obtained show similar trend of inhibition efficiency to that obtained from polarization curves measurements. This indicates that the type of the acid anions influences the corrosion process [21, 22]. Since, the ideal double layer capacitance, C, or none ideal double layer capacitance, Q, can be expressed in the Helmholtz model [18]. The lower value of Q_{dl} for HCl indicate that the Cl^- is specifically adsorbed on the metal surface. Further decrease in Q_{dl} on adding Mn_2O_3 nanoparticles indicates that the nanoparticles is also adsorbed through competitive or cooperative mechanism leading to formation of protective film. It is clearly observed that the Q_{dl} in the presence of the nanoparticles are arranged in the order Q_{dl}(HCl) < Q_{dl}(H_3PO_4l) < Q_{dl}(H_2SO_4). Therefore, the inhibition efficiency of nanoparticles in HCl should be the highest and that in H_2SO_4 is the lowest.

3.4. Inhibition mechanism

The enhancement of the corrosion resistance of metals depends on the nature of the metal surface, the structural and electronic characteristics of the nanoparticles, and the aggressive media. In acidic solution, Mn_2O_3 nanoparticles are reduced to Mn^2 according to the following equation [23]:

$Mn_2O_3 + 6\ H^+ + e \rightleftharpoons 2\ Mn^{2+} + 3\ H_2O$

Therefore, the metal protection could be attributed to the adsorption or electrodeposition reaction of metallic cations, manganese ions, on the mild steel surface. The adsorbed cations act as a protective layer, reducing the interaction between the aggressive ions and the steel surface.

4. CONCLUSIONS

The following conclusions can be summarized:

1. Mn_2O_3 nanoparticle synthesized by co-precipitation method at pH 10 enhance the corrosion resistance of mild steel in hydrochloric acid media.
2. Mn_2O_3 nanoparticle enhances the corrosion resistance of mild steel.
3. The inhibition efficiency of the studied nanoparticles in various acid medium follow the order 0.5 M HCl > 0.5 M H_3PO_4 > 0.5 M H_2SO_4 indicating that the type of the acid anions influences the corrosion process.

References

1. P.M. Wadhwania, D.G. Ladhaa, V.K. Panchal, and N.K. Shah, *RSC Adv*., 5 (2015) 7098.
2. M. Salavati-Niasari, N. Mir, and F.Davar, *Polyhedron*., 28 (2009) 1111.
3. H. Sachdeva, D. Dwivedi, R. Bhattacharjee, S. Khaturia, and R. Saroj, *J. Chem*.,10 (2013) 1.
4. M. Wu, J. Gao, S. Zhang, and A. chen, *J. Power Sources*., 159 (2006) 365.
5. S.R. Krishnakumar, M.Liberati, C. Grazioli, and C. Carbone, *J. Magn. Magn. Mater.*, 310 (2007) 8.
6. S.K. Dhoke, A.S.Khanna, T. Jai, and M. Sinha, *Prog. Org. Coat*., 64 (2009) 371.
7. I.B Obot, S. Umoren, and A. Johnson, *J. Mater. Environ. Sci.*, 4 (2013) 1013.
8. M.I. Zaki, M.A. Hasan, and L. Pasupulety, *Appl. Catal*., 198 (2000) 247.
9. M. Baldi, V.S. Escribano, J.M.G. Amores, F. Milella, and G. Busca, *Appl. Catal. B Environ*., 17 (1998) 175.
10. R.Talebi, *J. Mater. Sci. : Mater. Electron*., 28 (2017) 8316.
11. F. S. de Souza, A. Spinelli, *Corros. Sci.* 51 (2009) 642.
12. J. Saranya, P. Sounthari, and S. Chitra, *J. Mater. Environ. Sci.*, 8 (2017) 370.
13. M. Yadav, R. R. Sinha, T.K. Sarkar, and E. Ebenso, *J. Mol. Liq*., 212 (2015) 686.
14. H. Lgaz, K. Subrahmanya Bhat, R.Salghi, Shubhalaxmi, S. Jodeh, M. Algarra, B. Hammouti, I. H. Ali, and A. Essamri, *J. Mol. Liq*., 238 (2017) 71.
15. M. Bouanis, M. Tourabi, A. Nyassi, A. Zarrouk, C. Jama, and F. Bentiss, *Appl. Surf. Sci*., 389 (2016) 952.
16. H.T. Rahal, A.M. Abdel-Gaber, R. Awad, *Anti-Corros Method M.:* DOI (10.1108/ACMM-02-2018-1900)
17. H. T. Rahal, A. M. Abdel-Gaber, R. Awad, *Int. J. Electrochem. Sci.*, 12(2017)10115-10128
18. A.M. Abdel-Gaber, and M. Saadawy, *Int. J. Electrochem. Sci*., 8 (2013) 2080.
19. W. Peipei, L. Caihong, G. Haiyan, J. Xuerong, W. Hongqiang, and L.Kaixing, *Powder Technol*.203 (2010) 315.
20. F. Mohandes, M. Salavati-niasari, and M. Rezaei, *J. Mater. Sci*., 26 (2015) 7013.
21. E.E. Oguzie, *Port. Electrochim. Acta*, 26 (2008) 303.
22. M. Lashgari , M.R. Arshadi, and M.J Biglar, *J. Iran. Chem. Soc*., 7(2010) 478.
23. W. M. Haynes, ed., CRC Handbook of Chemistry and Physics, 96th Edition (Internet Version 2016), CRC Press/Taylor and Francis, Boca Raton, FL.